Nano Research 2016, 9(10): 3152–3161
DOI 10.1007/s12274-016-1197-4
Research Article
ISSN 1998-0124
CN 11-5974/O4

Dehydrated layered double hydroxides: Alcohothermal synthesis and oxygen evolution activity

Zhiyi Lu[1], Li Qian[1], Wenwen Xu[1], Yang Tian[1], Ming Jiang[1], Yaping Li[1], Xiaoming Sun[1,2] (✉), and Xue Duan[1]

[1] *State Key Laboratory of Chemical Resource Engineering, Beijing University of Chemical Technology, Beijing 100029, China*
[2] *Institute for New Energy Materials and Low-Carbon Technologies, Tianjin University of Technology, Tianjin 300384, China*

Received: 31 May 2016
Revised: 2 July 2016
Accepted: 3 July 2016

KEYWORDS
layered double hydroxides, alcohothermal synthesis, oxygen evolution reaction, dehydrated structure

ABSTRACT

Layered double hydroxides (LDHs) are a class of two-dimensional (2D) layered materials with extensive applications and well-developed synthesizing methods in aqueous media. In this work, we introduce an alcohothermal synthesis method for fabricating NiFe-LDHs with dehydrated galleries. The proposed process involves incomplete hydrolysis of urea for the simultaneous precipitation of metal ions, with the resulting water-deficient ethanol environment leading to the formation of a dehydrated structure. The formation of a gallery-dehydrated layer structure was confirmed by X-ray diffraction (XRD), as well as by a subsequent rehydration process. The methodology introduced here is also applicable for fabricating Fe-based LDHs (NiFe-LDH and NiCoFe-LDH) nanoarrays, which cannot be produced under the same conditions in aqueous media because of the different precipitation processes involved. The LDH nanoarrays exhibit excellent electrocatalytic performance in the oxygen evolution reaction, as a result of their high intrinsic activity and unique structural features. In summary, this study not only introduces a new method for synthesizing LDH materials, but also provides a new route towards highly active and robust electrodes for electrocatalysis.

1 Introduction

Layered double hydroxides (LDHs) with a brucite-like layer structure are an important family of two-dimensional (2D) anionic clay materials [1, 2]. The general formula of LDHs is $[M^{II}_{1-x}M^{III}_{x}(OH)_2]^{x+}(A^{n-})_{x/n}\cdot yH_2O$, where the identities of the divalent and trivalent cations (M^{II} and M^{III}, respectively), the interlayer anion (A^{n-}), and the stoichiometric coefficient (x) may be varied over a wide range [3]. Due to their unique crystal structure and large flexibility, LDHs have been actively investigated in a variety of fields, including catalysis [4, 5], flame retardation [6], biomaterials [7–9], photochemistry [10], and electrochemistry [11–13]. For instance, intercalation of photofunctional molecules as guest anions into LDH hosts creates a homogeneous

Address correspondence to sunxm@mail.buct.edu.cn

distribution of the photofunctional molecules, which suppresses their aggregation and thereby enhances the luminescence efficiency and photostability [14, 15]. Furthermore, partial substitution of Ni^{2+} by Fe^{3+} to form NiFe-LDHs leads to a unique electronic structure of the laminate, which results in an extraordinary catalytic activity for the oxygen evolution reaction (OER) [16–21].

LDHs can be synthesized by numerous techniques, the most common of which is the simple coprecipitation in aqueous media, which allows the one-pot synthesis of LDHs with a tunable content of intralayer cations and interlayer anions [22, 23]. Other methodologies, including ion-exchange [24], hydrothermal [25], and electrochemical [26] methods, have also proven effective for the fabrication of LDHs. The synthesis of LDHs is usually carried out in pure aqueous solutions [27–30]. Even though LDHs with unique morphologies have been obtained in partially aqueous solutions, their crystal structures are essentially the same [31–33]. Thus, there is significant interest in the development of synthesis methods for LDHs in non-aqueous media and in the investigation of the possible effects of different synthetic approaches on the properties of the LDHs.

In this work, a simple alcohothermal synthesis for fabricating LDHs was demonstrated. By simply mixing metal (e.g., Ni and Fe) nitrates with crystal waters and urea in pure ethanol followed by an alcohothermal process, NiFe-LDH intercalated with a majority of CO_3^{2-} and a minority of CNO^- anions could be readily formed. Notably, the ethanol-mediated NiFe-LDH (E-NiFe-LDH) exhibited an unusual interlayer spacing of ~0.71 nm, which is much narrower than that of conventional NiFe-LDHs (~0.79 nm) synthesized by coprecipitation in aqueous solution (A-NiFe-LDH), as illustrated in Fig. 1(a). This difference suggests that the E-NiFe-LDHs exhibit dehydrated galleries, possibly due to the absence of water during the synthesis. The interlayer spacing of E-NiFe-LDH was expanded upon exposure to a solution containing NaOH and Na_2CO_3, further confirming the formation of a gallery-dehydrated layer structure. The alcohothermal synthesis was also found to be effective for assembling dehydrated Fe-based LDHs (both binary E-NiFe-LDH and ternary E-NiCoFe-LDH) as nanoplate arrays (NPAs) on carbon fiber paper (CFP), which is difficult to achieve in aqueous solution due to the different precipitation conditions. Moreover, favored by their high intrinsic activity and unique structural features, the binary and ternary LDH NPAs exhibited outstanding performance (~300 mV for 200 $mA \cdot cm^{-2}$) and impressive durability as integrated electrodes for the OER, superior to the noble metal catalyst benchmark (Ir/C).

2 Results and discussion

The E-NiFe-LDHs were synthesized by a one-step alcohothermal route carried out in a pure ethanol medium containing $Ni(NO_3)_2 \cdot 6H_2O$, $Fe(NO_3)_3 \cdot 9H_2O$, and urea. The brown product obtained by this process was firstly examined through its X-ray diffraction (XRD) pattern, shown in Fig. 1(b). Compared with the A-NiFe-LDH (red line), which showed a series of Bragg reflections consistent with the well-known structure of NiFe-LDH intercalated by CO_3^{2-} (JCPDF: 51-0463) [34, 35], the (003) and (006) peak positions of E-NiFe-LDH were both shifted to substantially larger 2θ values (black line), indicating a change in the interlayer spacing (d_{003}). Specifically, d_{003} decreased from ~0.79 nm (A-NiFe-LDH) to ~0.71 nm (E-NiFe-LDH), denoting a collapsed LDH structure possibly produced by the lack of interlayer water [36–38].

Closer inspection of the FT-IR spectra (Fig. 1(c)) revealed a weaker bending vibration of interlayer water (~1,625 cm^{-1}) [39] for E-NiFe-LDH (black line), indicating a lower number of water molecules in the interlayer galleries and further confirming the formation of a dehydrated layer structure. Compared with A-NiFe-LDH (red line), E-NiFe-LDH exhibited a new adsorption peak at ~2,205 cm^{-1}, attributed to the symmetrical stretching mode of CNO^- [40]. Since the strength of the CO_3^{2-} peak (~1,385 cm^{-1}) was similar to that of the same peak in A-NiFe-LDH, while the CNO^- peak intensity was much weaker than the one reported for CNO^--intercalated LDHs [40], we infer that the E-NiFe-LDH was intercalated with a majority of CO_3^{2-} and a minority of CNO^- anions. Previous studies reported that LDHs intercalated with CO_3^{2-} or CNO^- possess similar d spacing (~0.79 nm) [40], suggesting that the possible contribution of CNO^-

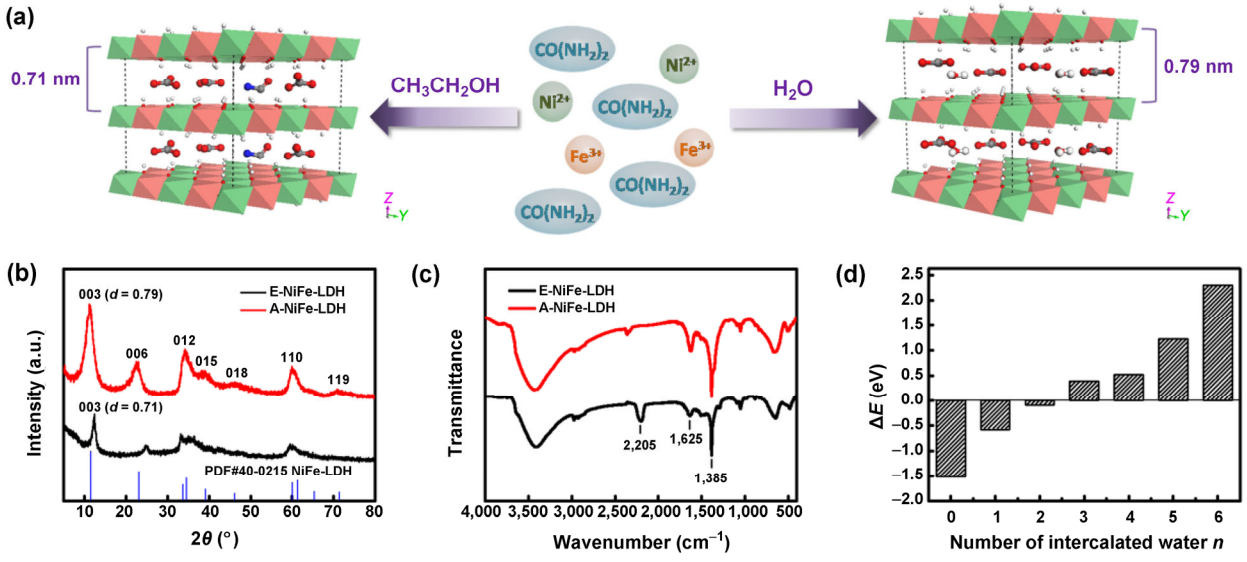

Figure 1 (a) Structural schemes of NiFe-LDHs synthesized in ethanol and aqueous media. E-NiFe-LDH shows a dehydrated structure with a narrower interlayer spacing compared with the NiFe-LDH fabricated by a conventional co-precipitation method (A-NiFe-LDH); (b) XRD patterns of E-NiFe-LDH (black curve) and A-NiFe-LDH (red curve). The A-NiFe-LDH pattern matches well with the typical NiFe-LDH profile (JCPDF: 40-0215), while an evident positive shift is observed for the (003) and (006) peaks of E-NiFe-LDH, indicating a narrower interlayer spacing for E-NiFe-LDH; (c) FT-IR patterns of E-NiFe-LDH and A-NiFe-LDH, indicating that A-NiFe-LDH is mainly intercalated with CO_3^{2-} with a minor content of CNO^- guest anions; (d) energy difference (ΔE) between two NiFe-LDHs (E-NiFe-LDH and A-NiFe-LDH, with interlayer spacing of 0.79 and 0.71 nm, respectively) containing different numbers of intercalated water molecules (n = 0–6). $\Delta E = E_E - E_A$, where E_E and E_A are the calculated energies of E-NiFe-LDH and A-NiFe-LDH, respectively. These results show that the NiFe-LDH with a narrower layer spacing (~0.71 nm) is thermodynamically more stable with lack of water.

doping to the observed decrease in d spacing can be ruled out.

Because the CNO^- and CO_3^{2-} anions could only originate from the transformation and hydrolysis of urea, we proposed a possible mechanism, described by the following chemical reactions, for the synthesis of dehydrated E-NiFe-LDH

$$2CH_3CH_2OH \longrightarrow CH_3CH_2OCH_2CH_3 + H_2O \quad (1)$$

$$CO(NH_2)_2 \longrightarrow NH_4CNO \quad (2)$$

$$NH_4CNO + 2H_2O \longrightarrow 2NH_4^+ + CO_3^{2-} \quad (3)$$

$$xNi^{2+} + yFe^{3+} + zOH^- + kCNO^- + uCO_3^{2-} \longrightarrow Ni_xFe_y(OH)_z(CNO)_k(CO_3)_u \quad (4)$$

Ethanol would first undergo the etherization Reaction (1), which produces a small amount of H_2O, as shown by gas chromatography-mass spectrometry (GC-MS, Fig. S1 in the Electronic Supplementary Material (ESM)). Then, the as-produced H_2O together with the crystal water of the metal nitrates would assist the hydrolysis of urea to form ammonium carbonate, as illustrated by Reactions (2) and (3) [22]. It should be noted that Reaction (3) would not proceed to completion because an insufficient amount of reactant water is produced from the starting materials and from Reaction (1). Since the hydrolysis degree of the carbonate is higher than that of ammonium ions, a small amount of hydroxyl ions would be produced from water. Finally, the coprecipitation Reaction (4) would occur to form E-NiFe-LDH and the water-deficient ethanol environment would produce a dehydrated structure.

Computer simulations were employed to confirm that the narrower d spacing observed for E-NiFe-LDH could be primarily attributed to the removal of interlayer water. The energies of NiFe-LDHs models with different interlayer spacings (0.71 and 0.79 nm) and various numbers of intercalated water molecules (n = 0–6) were calculated by the DFT+U method. The calculated energy difference is shown in Fig. 1(d) (the specific energies of NiFe-LDHs with different layer

spacings are summarized in Table S1 in the ESM). The figure highlights that when the number of intercalated water molecules was larger than 2, the NiFe-LDH with a larger layer spacing had lower energy. In contrast, for n = 0 or 1 the energy of the NiFe-LDH with narrower interlayer spacing was lower. Therefore, a narrower layer spacing (0.71 nm) was thermodynamically more stable in the case of the dehydrated LDHs.

Furthermore, it was found that the E-NiFe-LDH with a dehydrated structure could absorb water into its galleries, resulting in an expansion of the interlayer spacing. The corresponding XRD pattern (Fig. S2 in the ESM) shows that, after immersion in an alkali solution with vigorous stirring for 1–2 days, the d_{003} parameter of E-NiFe-LDH increased back to its normal value of ~0.79 nm, indicating the successful intercalation of water molecules. The occurrence of this rehydration process [41, 42] further supports the dehydrated structure of E-NiFe-LDH.

The rehydration of E-NiFe-LDH was accompanied by morphological changes [43]. The morphologies of E-NiFe-LDH before and after rehydration were examined by both scanning and transmission electron microscopy (SEM and TEM, respectively), as shown in Fig. 2.

The E-NiFe-LDH showed a flower-like nanostructure composed of many interpenetrated nanoplates with an average size of ~1 μm, whereas only individual nanoplates could be observed in the sample after rehydration (Figs. 2(a) and 2(c)). The TEM images (Fig. 2(b)) show that the thickness of the interpenetrated nanoplates was only ~3.6 nm, similar to that of the nanoplates after rehydration (Fig. 2(d)). Hence, we hypothesize that the rehydration process broke the nanoflowers into nanoplates (Fig. 2(e)).

The present alcohothermal method assisted by urea hydrolysis could also be applied for fabricating E-NiFe-LDH NPAs by simply incorporating a carbon substrate (CFP) into the reaction synthesis, as schematically shown in Fig. 3(a). CFP was chosen as substrate because of its high porosity and conductivity, which helped to increase the active surface area and enhance the electrocatalytic performance [44]. Unlike the smooth surface (Fig. S3 in the ESM), after alcohothermal growth the CFP substrate was uniformly

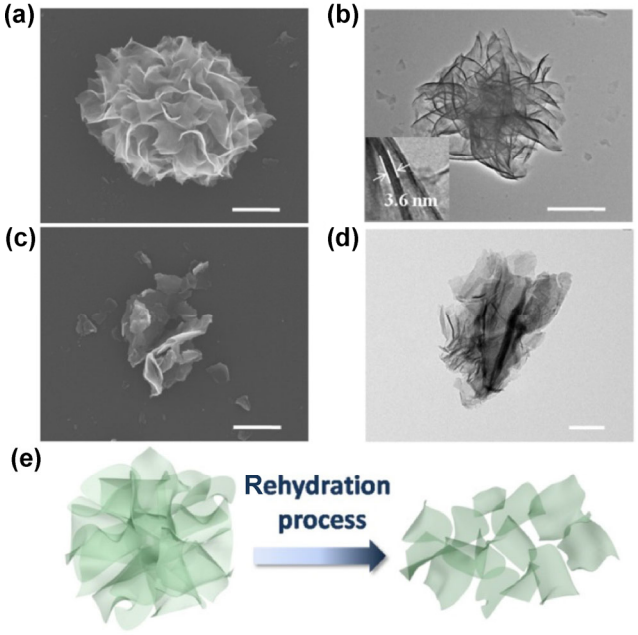

Figure 2 (a) and (b) Typical SEM and TEM images of E-NiFe-LDH, showing a flower-like structure comprising many interpenetrated nanoplates (inset: magnified TEM image of E-NiFe-LDH, highlighting a small thickness of ~3.6 nm for the nanoplates); (c) and (d) SEM and TEM images of E-NiFe-LDH after the rehydration process, revealing a nanoplate (rather than nanoflower) structure (inset: magnified TEM image of E-NiFe-LDH after rehydration, highlighting a thickness similar to that of the interpenetrated E-NiFe-LDH nanoplates); (e) schematic illustration of the breaking process of E-NiFe-LDH nanoflowers in the rehydration process. The scale bars are 1 μm (a)–(c) and 200 nm (d).

and densely covered by vertically aligned nanoplates (Fig. 3(b)), resulting in an oriented and rigid three-dimensional (3D) architecture. High-magnification SEM images (Fig. 3(c)) further revealed the size (0.5–1 μm) and thickness (<5 nm) of the nanoplates, which matched well with the corresponding parameters of E-NiFe-LDH. The co-existence of both Ni and Fe elements was confirmed by energy dispersive spectroscopy (EDS) data (Table S2 in the ESM). The XRD patterns of E-NiFe-LDH and E-NiCoFe-LDH NPAs (black line in Fig. 3(d)) showed strong peaks corresponding to the carbon substrate (marked with "#") and minor peaks that could be indexed to the dehydrated LDH structure.

On the other hand, only nanowires, rather than nanoplates, were observed when the growth process was performed in aqueous solution (Fig. S4(a) in the ESM). Additional characterizations (Fig. S4(b) and Table S2 in the ESM) revealed that the nanowires

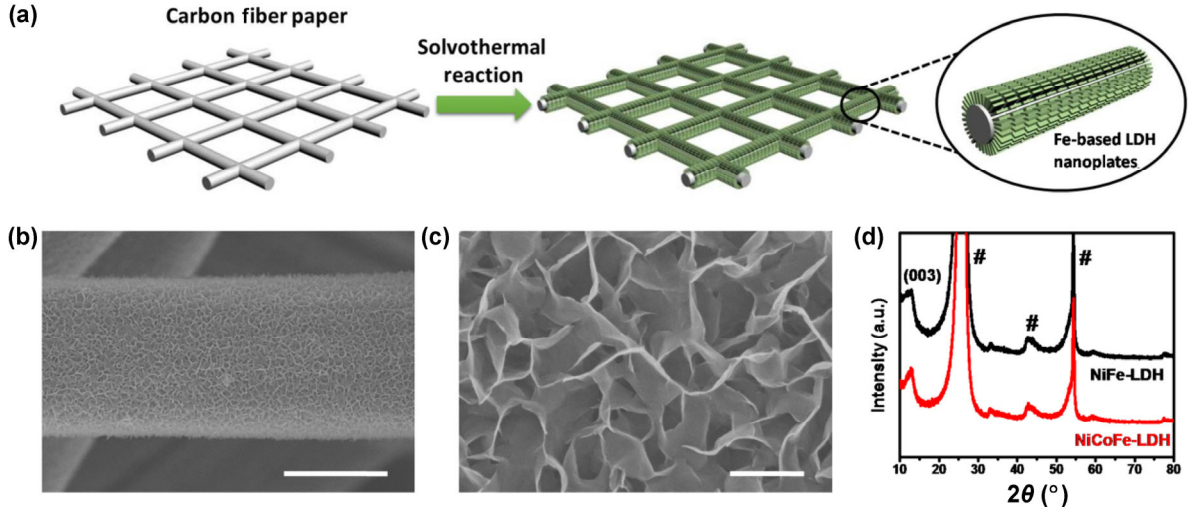

Figure 3 (a) Schematic illustration of the growth process of Fe-based LDH NPAs after the solvothermal process; (b) and (c) low- and high-magnification SEM images of typical E-NiFe-LDH NPAs (scale bar: 5 μm and 500 nm for (b) and (c), respectively); (d) XRD patterns of E-NiFe-LDH and E-NiCoFe-LDH NPAs on carbon fiber paper (the peaks marked with "#" correspond to the carbon substrate). These results demonstrate that Fe-based LDH nanoplate arrays can be successfully fabricated by the present alcohothermal method.

mainly consisted of nickel hydroxide carbonates with negligible iron content. This difference could be explained by the different precipitation processes involved in each case. The K_{sp} value of $Ni(OH)_2$ in aqueous solution at room temperature is ~2.0×10^{-14}, much larger than that of $Fe(OH)_3$ (~4.0×10^{-38}). As a result, the precipitation of Fe^{3+} ions is thermodynamically easier than that of Ni^{2+} ions.

The required pH values for precipitating Fe^{3+} and Ni^{2+} (at a concentration of 0.01 M) are ~2.2 and ~6.4, respectively. Thus, we can hypothesize that the nucleation of $Fe(OH)_3$ mostly occurred before the hydrothermal process (the initial pH value was ~5), while that of $Ni_2(OH)_2CO_3$ took place on the carbon fiber substrates during the hydrolysis of urea. Accordingly, the $Fe(OH)_3$ nuclei formed in solution rather than on the CFP surface, resulting in the absence of Fe in the final product. In fact, when the hydrothermal reaction was conducted in aqueous solution with a pure Fe salt, only a small amount of nanoparticles were formed on the CFP (Fig. S5 in the ESM), thereby confirming the above hypothesis. Therefore, we suggest that Ni and Fe have a similar precipitation behavior in ethanol solution, which results in homogeneous nucleation and precipitation processes.

Further experiments indicated that, in addition to the binary E-NiFe-LDH, ternary E-NiCoFe-LDH NPAs with a dehydrated layer structure and similar morphology could also be fabricated (red line in Fig. 3(d) and Fig. S6 in the ESM), highlighting the general efficacy of this method. The Ni:Co:Fe ratio was 2:1:1, according to the EDS data listed in Table S2 (in the ESM).

Previous investigations showed that marked improvement in the electrochemical properties of LDHs could be achieved through appropriate structural modifications [45–49]. The OER activity of A-NiFe-LDH and E-NiFe-LDH powders, examined in Fig. S7 (in the ESM), shows that although E-NiFe-LDH was not as OER-active as A-NiFe-LDH, it can be activated even better after the rehydration process. This may be due to the larger interlayer spacing of A-NiFe-LDH (0.79 nm) compared to that of E-NiFe-LDH (0.71 nm), which facilitates the electrolyte penetration. However, the rehydration process led to a smaller size of the nanoplates and to a larger interlayer spacing, resulting in a marked improvement in the OER performance. It should be noted that the OER performance of E-NiFe-LDH would be activated during cycling testing, indicating that the rehydration process could occur *in situ* while testing the OER performance.

Figures 4(a) and 4(b) show the stabilized OER performances of the E-NiFe-LDH and E-NiCoFe-LDH NPAs under the same conditions. The E-NiFe-LDH NPAs showed an onset potential (defined as the starting point of the linear range in the Tafel plot) of ~1.49 V vs. reversible hydrogen electrode (RHE) and an overpotential of ~310 mV at ~25 mA·cm^{-2} (η_{25}). Incorporating a small amount of Co further reduced both onset potential and η_{25} to 1.46 V and ~295 mV, respectively. Both E-NiFe-LDH and E-NiCoFe-LDH NPAs outperformed a commercial Ir/C catalyst with the same mass loading. The Tafel slopes of both electrodes were similar and close to 40 mV·dec^{-1}, which indicates a mechanism involving a pre-equilibrium consisting of a one-electron electrochemical step with a possible chemical step, followed by a one-electron electrochemical rate-determining step [50]. A negligible current response was observed for pure CFP (less than 1 mA·cm^{-2} at 1.6 V), thus ruling out the possible current contribution from the substrate.

Since the fabricated E-NiFe-LDH and E-NiCoFe-LDH NPAs exhibited very similar morphologies and sizes, their different catalytic activity might be related to the different transition metal composition.

The above electrochemical results clearly demonstrate that NiFe-LDH was already active for the OER, and a small amount of Co substitution for Ni could further improve the overall performance. It has been reported that Fe-doped nickel matrices (oxides [51, 52], hydroxides [16], and oxyhydroxides [53]) could significantly reduce the onset overpotential and accelerate the OER kinetics, which could be explained by the enhanced conductivity and partial charge transfer between Ni and Fe [53]. Moreover, doping a small amount of Co into mixed metal oxides containing Ni and Fe could facilitate the formation of a more conductive NiOOH phase and induce strain effects, resulting in enhanced OER activity [54]. A significant work highlighted the excellent OER activity of amorphous NiCoFe oxides prepared by a photochemical route [55]. Thus, by virtue of the synergistic effect of the transition metals, the present E-NiCoFe-LDH NPAs should represent attractive and promising water oxidation electrodes.

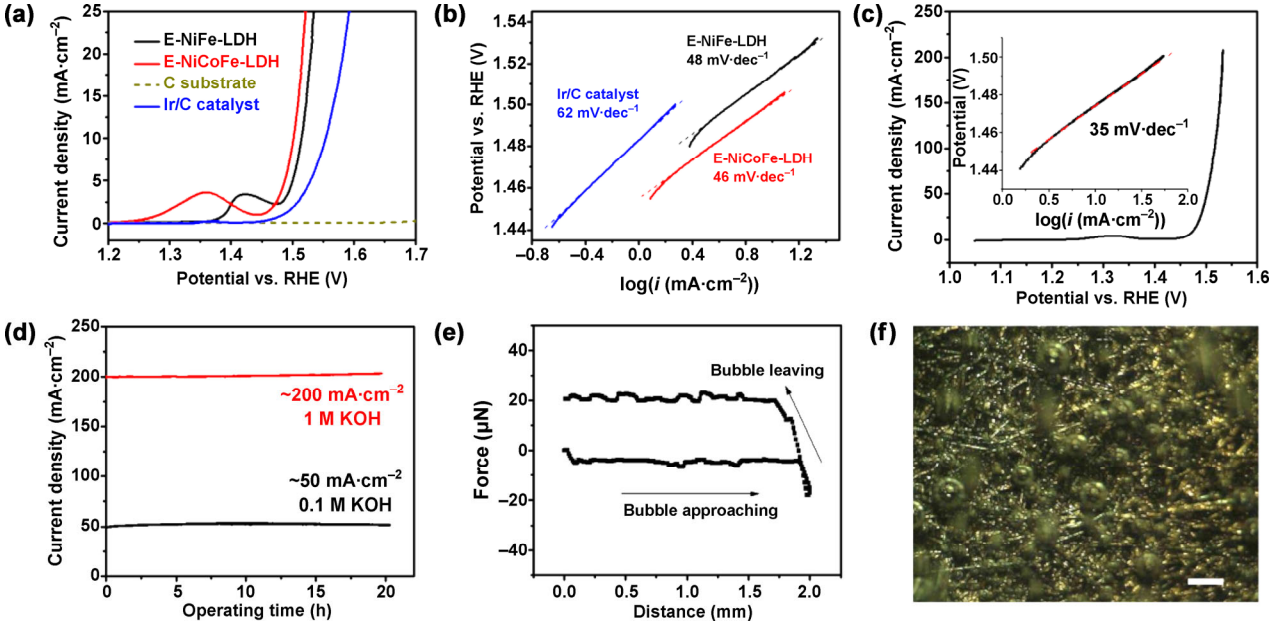

Figure 4 (a) Polarization curves of E-NiFe-LDH and E-NiCoFe-LDH NPAs, commercial Ir/C catalyst, and pure carbon substrate. Both LDH NPAs show a lower onset potential and a faster current density increase than the Ir/C catalyst; (b) corresponding Tafel plots of the three catalysts; (c) polarization curve of NiCoFe-LDH NPAs in 1 M KOH electrolyte (the inset shows the corresponding Tafel plot); (d) stability testing of NiCoFe-LDH NPAs at high current densities in both 0.1 and 1 M KOH electrolytes; (e) adhesion force between the E-NiCoFe-LDH NPAs electrode surface and a single gas bubble. The negligible response indicates a weak interaction; (f) optical image of oxygen gas bubble release on the E-NiCoFe-LDH NPAs electrode surface; the size of the releasing gas bubbles is in the range of 100–200 μm in diameter, and the scale bar is 200 μm.

The industrial applicability of these systems was demonstrated by testing the E-NiCoFe-LDH electrode in 1 M KOH electrolyte in order to achieve a current density of hundreds of milliamperes per square centimeter, due to the high conductivity of the electrolyte. As expected, this E-NiCoFe-LDH NPA showed a further improvement in the OER performance, with a lower Tafel slope (~35 $mV \cdot dec^{-1}$) and a much higher current density (~200 $mA \cdot cm^{-2}$) at a potential of 1.53 V, as shown in Fig. 4(c). Moreover, since a carbon substrate is employed in our approach, the long-term stability should be an essential aspect in the catalyst evaluation because carbon would be probably corroded [56] and thus lead to easy detachment of the catalyst film. The stability of the E-NiCoFe-LDH NPAs was thus examined, as illustrated in the current density vs. time plots in Fig. 4(d). Under constant overpotentials, stable OER current densities (~50 and ~200 $mA \cdot cm^{-2}$ for 0.1 and 1 M KOH electrolytes, respectively) were observed on this self-supported 3D electrode, with negligible degradations after more than 20 h of testing, revealing an excellent stability. This might be due to the uniform coating of the E-NiCoFe-LDH nanoplates, which served as a good protection for the carbon substrate.

Besides the intrinsically high activity of the E-NiCoFe-LDHs, the outstanding OER performance of these systems could be attributed to their unique structural features. Similar 3D architectures have proven ideal for lithium ion batteries and supercapacitors [57–61]. These devices benefit from the intimate contact with the current collector, as well as from their nanosized units, high porosity, and high surface area, which permit a direct pathway for electron transport, shorten the diffusion length for electrolyte penetration, and eliminate the polymer binders that would induce additional resistance.

More importantly, this 3D architecture would provide low adhesion for the as-formed gas bubbles, thus promoting their release and keeping the working efficiency constant [62–64]. The adhesion force measurements highlighted a negligible gas bubble adhesion of E-NiCoFe-LDH NPAs (Fig. 4(e)), and the adhesion force curves at different positions further confirmed the uniformity of the electrode surface (Fig. S8 in the ESM). Consequently, the size of the releasing gas bubbles was only 100–200 μm in diameter (Fig. 4(f)), which in turn accelerated the gas bubble release. Accordingly, the fast removal of the as-formed gas bubbles could maximize the exposure of active areas to the electrolyte and minimize the negative effects induced by the bubble adhesion, thus leading to a fast current increase and creating a stable working condition [63].

3 Summary

In summary, this work demonstrated a non-aqueous approach for fabricating LDHs. Using ethanol as the only solvent, gallery-dehydrated E-NiFe-LDH with a reduced interlayer spacing (~0.71 nm) could be obtained through an alcohothermal process assisted by urea hydrolysis. The interlayer spacing of the E-NiFe-LDHs was found to expand after a subsequent rehydration process, thus confirming the formation of a dehydrated structure. The present ethanol-mediated synthesis method could be further employed for the efficient fabrication of Fe-based dehydrated LDH NPAs, including E-NiFe-LDH and E-NiCoFe-LDH. However, nanoarrays could not be prepared in aqueous solution because of the different nucleation processes involved. Both E-NiFe-LDH and E-NiCoFe-LDH exhibited excellent performance and stability as integrated electrodes for the OER, superior to the commercial Ir/C catalyst. This first demonstration of the non-aqueous fabrication and application of LDHs may have a deep impact into guiding future investigations on the synthesis of these systems.

Acknowledgements

This work was support by the National Natural Science Foundation of China, the Program for Changjiang Scholars and Innovative Research Team in the University, and the Fundamental Research Funds for the Central Universities, and the long-term subsidy mechanism from the Ministry of Finance and the Ministry of Education of PRC.

Electronic Supplementary Material: Supplementary material (experimental details and supplementary figures) is available in the online version of this article at http://dx.doi.org/10.1007/s12274-016-1197-4.

References

[1] Evans, D. G.; Duan, X. Preparation of layered double hydroxides and their applications as additives in polymers, as precursors to magnetic materials and in biology and medicine. *Chem. Commun.* **2006**, 485–496.

[2] Wang, Q.; O'Hare, D. Recent advances in the synthesis and application of layered double hydroxide (LDH) nanosheets. *Chem. Rev.* **2012**, *112*, 4124–4155.

[3] Guo, X. X.; Zhang, F. Z.; Evans, D. G.; Duan, X. Layered double hydroxide films: Synthesis, properties and applications. *Chem. Commun.* **2010**, *46*, 5197–5210.

[4] Fan, G. L.; Li, F.; Evans, D. G.; Duan, X. Catalytic applications of layered double hydroxides: Recent advances and perspectives. *Chem. Soc. Rev.* **2014**, *43*, 7040–7066.

[5] Feng, J. T.; He, Y. F.; Liu, Y. R.; Du, Y. Y.; Li, D. Q. Supported catalysts based on layered double hydroxides for catalytic oxidation and hydrogenation: General functionality and promising application prospects. *Chem. Soc. Rev.* **2015**, *44*, 5291–5319.

[6] Huang, G. B.; Fei, Z. D.; Chen, X. Y.; Qiu, F. L.; Wang, X.; Gao, J. R. Functionalization of layered double hydroxides by intumescent flame retardant: Preparation, characterization, and application in ethylene vinyl acetate copolymer. *Appl. Surf. Sci.* **2012**, *258*, 10115–10122.

[7] Choy, J. H.; Choi, S. J.; Oh, J. M.; Park, T. Clay minerals and layered double hydroxides for novel biological applications. *Appl. Clay Sci.* **2007**, *36*, 122–132.

[8] Li, L.; Gu, W. Y.; Liu, J.; Yan, S. Y.; Xu, Z. P. Amine-functionalized SiO_2 nanodot-coated layered double hydroxide nanocomposites for enhanced gene delivery. *Nano Res.* **2015**, *8*, 682–694.

[9] Carja, G.; Grosu, E. F.; Petrarean, C.; Nichita, N. Self-assemblies of plasmonic gold/layered double hydroxides with highly efficient antiviral effect against the hepatitis B virus. *Nano Res.* **2015**, *8*, 3512–3523.

[10] Yan, D. P.; Lu, J.; Wei, M.; Han, J. B.; Ma, J.; Li, F.; Evans, D. G.; Duan, X. Ordered poly(p-phenylene)/layered double hydroxide ultrathin films with blue luminescence by layer-by-layer assembly. *Angew. Chem., Int. Ed.* **2009**, *48*, 3073–3076.

[11] Qian, L.; Lu, Z. Y.; Xu, T. H.; Wu, X. C.; Tian, Y.; Li, Y. P.; Huo, Z. Y.; Sun, X. M.; Duan, X. Trinary layered double hydroxides as high-performance bifunctional materials for oxygen electrocatalysis. *Adv. Energy Mater.* **2015**, *5*, 1500245.

[12] Wu, J.; Ren, Z. Y.; Du, S. C.; Kong, L. J.; Liu, B. W.; Xi, W.; Zhu, J. Q.; Fu, H. G. A highly active oxygen evolution electrocatalyst: Ultrathin CoNi double hydroxide/CoO nanosheets synthesized via interface-directed assembly. *Nano Res.* **2016**, *9*, 713–725.

[13] Wang, Z.; Jia, W.; Jiang, M. L.; Chen, C.; Li, Y. D. Microwave-assisted synthesis of layer-by-layer ultra-large and thin NiAl-LDH/RGO nanocomposites and their excellent performance as electrodes. *Sci. China Mater.* **2015**, *58*, 944–952.

[14] Yan, D. P.; Lu, J.; Ma, J.; Qin, S. H.; Wei, M.; Evans, D. G.; Duan, X. Layered host–guest materials with reversible piezochromic luminescence. *Angew. Chem., Int. Ed.* **2011**, *50*, 7037–7040.

[15] Yan, D. P.; Lu, J.; Wei, M.; Evans, D. G.; Duan, X. Recent advances in photofunctional guest/layered double hydroxide host composite systems and their applications: Experimental and theoretical perspectives. *J. Mater. Chem.* **2011**, *21*, 13128–13139.

[16] Gong, M.; Li, Y. G.; Wang, H. L.; Liang, Y. Y.; Wu, J. Z.; Zhou, J. G.; Wang, J.; Regier, T.; Wei, F.; Dai, H. J. An advanced Ni-Fe layered double hydroxide electrocatalyst for water oxidation. *J. Am. Chem. Soc.* **2013**, *135*, 8452–8455.

[17] Long, X.; Li, J. K.; Xiao, S.; Yan, K. Y.; Wang, Z. L.; Chen, H. N.; Yang, S. H. A strongly coupled graphene and FeNi double hydroxide hybrid as an excellent electrocatalyst for the oxygen evolution reaction. *Angew. Chem., Int. Ed.* **2014**, *53*, 7584–7588.

[18] Song, F.; Hu, X. L. Exfoliation of layered double hydroxides for enhanced oxygen evolution catalysis. *Nat. Commun.* **2014**, *5*, 4477.

[19] Luo, J. S.; Im, J.-H.; Mayer, M. T.; Schreier, M.; Nazeeruddin, M. K.; Park, N.-G.; Tilley, S. D.; Fan, H. J.; Grätzel, M. Water photolysis at 12.3% efficiency via perovskite photovoltaics and earth-abundant catalysts. *Science* **2014**, *345*, 1593–1596.

[20] Gong, M.; Dai, H. J. A mini review of NiFe-based materials as highly active oxygen evolution reaction electrocatalysts. *Nano Res.* **2015**, *8*, 23–39.

[21] Gong, M.; Wang, D.-Y.; Chen, C.-C.; Hwang, B.-J.; Dai, H. J. A mini review on nickel-based electrocatalysts for alkaline hydrogen evolution reaction. *Nano Res.* **2016**, *9*, 28–46.

[22] He, J.; Wei, M.; Li, B.; Kang, Y.; Evans, D. G.; Duan, X. Preparation of layered double hydroxides. In *Layered Double Hydroxides*; Duan, X.; Evans, D. G., Eds.; Springer: Berlin Heidelberg, 2006; pp 89–119.

[23] Zhao, Y.; Li, F.; Zhang, R.; Evans, D. G.; Duan, X. Preparation of layered double-hydroxide nanomaterials with a uniform crystallite size using a new method involving separate nucleation and aging steps. *Chem. Mater.* **2002**, *14*, 4286–4291.

[24] Morel-Desrosiers, N.; Pisson, J.; Israëli, Y.; Taviot-Guého, C.; Besse, J. P.; Morel, J. P. Intercalation of dicarboxylate anions into a Zn-Al-Cl layered double hydroxide: Microcalorimetric determination of the enthalpies of anion exchange. *J. Mater. Chem.* **2003**, *13*, 2582–2585.

[25] Oh, J. M.; Hwang, S. H.; Choy, J. H. The effect of synthetic conditions on tailoring the size of hydrotalcite particles. *Solid State Ionics* **2002**, *151*, 285–291.

[26] Prevot, V.; Forano, C.; Khenifi, A.; Ballarin, B.; Scavetta, E.; Mousty, C. A templated electrosynthesis of macroporous NiAl layered double hydroxides thin films. *Chem. Commun.* **2011**, *47*, 1761–1763.

[27] Forticaux, A.; Dang, L. N.; Liang, H. F.; Jin, S. Controlled synthesis of layered double hydroxide nanoplates driven by screw dislocations. *Nano Lett.* **2015**, *15*, 3403–3409.

[28] Liang, H. F.; Meng, F.; Cabán-Acevedo, M.; Li, L. S.; Forticaux, A.; Xiu, L. C.; Wang, Z. C.; Jin, S. Hydrothermal continuous flow synthesis and exfoliation of NiCo layered double hydroxide nanosheets for enhanced oxygen evolution catalysis. *Nano Lett.* **2015**, *15*, 1421–1427.

[29] Liu, Z. P.; Ma, R. Z.; Osada, M.; Iyi, N.; Ebina, Y.; Takada, K.; Sasaki, T. Synthesis, anion exchange, and delamination of Co-Al layered double hydroxide: Assembly of the exfoliated nanosheet/polyanion composite films and magneto-optical studies. *J. Am. Chem. Soc.* **2006**, *128*, 4872–4880.

[30] Ma, R. Z.; Liu, Z. P.; Takada, K.; Iyi, N.; Bando, Y.; Sasaki, T. Synthesis and exfoliation of Co^{2+}-Fe^{3+} layered double hydroxides: An innovative topochemical approach. *J. Am. Chem. Soc.* **2007**, *129*, 5257–5263.

[31] Hu, G.; O'Hare, D. Unique layered double hydroxide morphologies using reverse microemulsion synthesis. *J. Am. Chem. Soc.* **2005**, *127*, 17808–17813.

[32] Yu, J. F.; Martin, B. R.; Clearfield, A.; Luo, Z. P.; Sun, L. Y. One-step direct synthesis of layered double hydroxide single-layer nanosheets. *Nanoscale* **2015**, *7*, 9448–9451.

[33] Chen, H.; Hu, L. F.; Chen, M.; Yan, Y.; Wu, L. M. Nickel–cobalt layered double hydroxide nanosheets for high-performance supercapacitor electrode materials. *Adv. Funct. Mater.* **2014**, *24*, 934–942.

[34] Lu, Z. Y.; Xu, W. W.; Zhu, W.; Yang, Q.; Lei, X. D.; Liu, J. F.; Li, Y. P.; Sun, X. M.; Duan, X. Three-dimensional NiFe layered double hydroxide film for high-efficiency oxygen evolution reaction. *Chem. Commun.* **2014**, *50*, 6479–6482.

[35] Tang, D.; Liu, J.; Wu, X. Y.; Liu, R. H.; Han, X.; Han, Y. Z.; Huang, H.; Liu, Y.; Kang, Z. H. Carbon quantum dot/NiFe layered double-hydroxide composite as a highly efficient electrocatalyst for water oxidation. *ACS Appl. Mater. Interfaces* **2014**, *6*, 7918–7925.

[36] Pérez-Ramírez, J.; Mul, G.; Kapteijn, F.; Moulijn, J. A. *In situ* investigation of the thermal decomposition of Co-Al hydrotalcite in different atmospheres. *J. Mater. Chem.* **2001**, *11*, 821–830.

[37] Kovanda, F.; Rojka, T.; Bezdička, P.; Jirátová, K.; Obalová, L.; Pacultová, K.; Bastl, Z.; Grygar, T. Effect of hydrothermal treatment on properties of Ni-Al layered double hydroxides and related mixed oxides. *J. Solid State Chem.* **2009**, *182*, 27–36.

[38] Kovanda, F.; Rojka, T.; Dobešová, J.; Machovič, V.; Bezdička, P.; Obalová, L.; Jirátová, K.; Grygar, T. Mixed oxides obtained from Co and Mn containing layered double hydroxides: Preparation, characterization, and catalytic properties. *J. Solid State Chem.* **2006**, *179*, 812–823.

[39] Lin, Y. J.; Li, D. Q.; Evans, D. G.; Duan, X. Modulating effect of Mg-Al-CO_3 layered double hydroxides on the thermal stability of PVC resin. *Polym. Degrad. Stabil.* **2005**, *88*, 286–293.

[40] Saber, O.; Hatano, B.; Tagaya, H. Controlling of the morphology of Co–Ti LDH. *Mater. Sci. Eng. C* **2005**, *25*, 462–471.

[41] Gennequin, C.; Cousin, R.; Lamonier, J. F.; Siffert, S.; Aboukais, A. Toluene total oxidation over Co supported catalysts synthesised using "memory effect" of Mg-Al hydrotalcite. *Catal. Commun.* **2008**, *9*, 1639–1643.

[42] Ferreira, O. P.; Alves, O. L.; Gouveia, D. X.; Souza Filho, A. G.; de Paiva, J. A. C.; Filho, J. M. Thermal decomposition and structural reconstruction effect on Mg-Fe-based hydrotalcite compounds. *J. Solid State Chem.* **2004**, *177*, 3058–3069.

[43] Pavel, O. D.; Bîrjega, R.; Che, M.; Costentin, G.; Angelescu, E.; Şerban, S. The activity of Mg/Al reconstructed hydrotalcites by “memory effect” in the cyanoethylation reaction. *Catal. Commun.* **2008**, *9*, 1974–1978.

[44] Wang, H. T.; Lu, Z. Y.; Kong, D. S.; Sun, J.; Hymel, T. M.; Cui, Y. Electrochemical tuning of MoS_2 nanoparticles on three-dimensional substrate for efficient hydrogen evolution. *ACS Nano* **2014**, *8*, 4940–4947.

[45] Faber, M. S.; Dziedzic, R.; Lukowski, M. A.; Kaiser, N. S.; Ding, Q.; Jin, S. High-performance electrocatalysis using metallic cobalt pyrite (CoS_2) micro- and nanostructures. *J. Am. Chem. Soc.* **2014**, *136*, 10053–10061.

[46] Chen, Z. B.; Cummins, D.; Reinecke, B. N.; Clark, E.; Sunkara, M. K.; Jaramillo, T. F. Core–shell MoO_3–MoS_2 nanowires for hydrogen evolution: A functional design for electrocatalytic materials. *Nano Lett.* **2011**, *11*, 4168–4175.

[47] Li, Y. G.; Hasin, P.; Wu, Y. Y. $Ni_xCo_{3-x}O_4$ nanowire arrays for electrocatalytic oxygen evolution. *Adv. Mater.* **2010**, *22*, 1926–1929.

[48] Wang, J.; Zhong, H.-X.; Qin, Y.-L.; Zhang, X.-B. An efficient three-dimensional oxygen evolution electrode. *Angew. Chem., Int. Ed.* **2013**, *52*, 5248–5253.

[49] Lu, Z. Y.; Wu, X. C.; Jiang, M.; Wang, J. N.; Liu, J. F.; Lei, X. D.; Sun, X. M. Transition metal oxides/hydroxides nanoarrays for aqueous electrochemical energy storage systems. *Sci. China Mater.* **2014**, *57*, 59–69.

[50] Castro, E. B.; Gervasi, C. A. Electrodeposited Ni-Co-oxide electrodes: Characterization and kinetics of the oxygen evolution reaction. *Int. J. Hydrogen Energy* **2000**, *25*, 1163–1170.

[51] Landon, J.; Demeter, E.; Inoğlu, N.; Keturakis, C.; Wachs, I. E.; Vasić, R.; Frenkel, A. I.; Kitchin, J. R. Spectroscopic characterization of mixed Fe-Ni oxide electrocatalysts for the oxygen evolution reaction in alkaline electrolytes. *ACS Catal.* **2012**, *2*, 1793–1801.

[52] Louie, M. W.; Bell, A. T. An investigation of thin-film Ni-Fe oxide catalysts for the electrochemical evolution of oxygen. *J. Am. Chem. Soc.* **2013**, *135*, 12329–12337.

[53] Trotochaud, L.; Young, S. L.; Ranney, J. K.; Boettcher, S. W. Nickel-iron oxyhydroxide oxygen-evolution electrocatalysts: The role of intentional and incidental iron incorporation. *J. Am. Chem. Soc.* **2014**, *136*, 6744–6753.

[54] Bates, M. K.; Jia, Q. Y.; Doan, H.; Liang, W. T.; Mukerjee, S. Charge-transfer effects in Ni-Fe and Ni-Fe-Co mixed-metal oxides for the alkaline oxygen evolution reaction. *ACS Catal.* **2016**, *6*, 155–161.

[55] Smith, R. D. L.; Prévot, M. S.; Fagan, R. D.; Zhang, Z. P.; Sedach, P. A.; Siu, M. K. J.; Trudel, S.; Berlinguette, C. P. Photochemical route for accessing amorphous metal oxide materials for water oxidation catalysis. *Science* **2013**, *340*, 60–63.

[56] Zhao, Y.; Nakamura, R.; Kamiya, K.; Nakanishi, S.; Hashimoto, K. Nitrogen-doped carbon nanomaterials as non-metal electrocatalysts for water oxidation. *Nat. Commun.* **2013**, *4*, 2390.

[57] Chabi, S.; Peng, C.; Hu, D.; Zhu, Y. Q. Ideal three-dimensional electrode structures for electrochemical energy storage. *Adv. Mater.* **2014**, *26*, 2440–2445.

[58] Ellis, B. L.; Knauth, P.; Djenizian, T. Three-dimensional self-supported metal oxides for advanced energy storage. *Adv. Mater.* **2014**, *26*, 3368–3397.

[59] Jiang, J.; Li, Y. Y.; Liu, J. P.; Huang, X. T.; Yuan, C. Z.; Lou, X. W. Recent advances in metal oxide-based electrode architecture design for electrochemical energy storage. *Adv. Mater.* **2012**, *24*, 5166–5180.

[60] Zhang, H. G.; Yu, X. D.; Braun, P. V. Three-dimensional bicontinuous ultrafast-charge and -discharge bulk battery electrodes. *Nat. Nanotechnol.* **2011**, *6*, 277–281.

[61] Chan, C. K.; Peng, H. L.; Liu, G.; McIlwrath, K.; Zhang, X. F.; Huggins, R. A.; Cui, Y. High-performance lithium battery anodes using silicon nanowires. *Nat. Nanotechnol.* **2008**, *3*, 31–35.

[62] Lu, Z. Y.; Sun, M.; Xu, T. H.; Li, Y. J.; Xu, W. W.; Chang, Z.; Ding, Y.; Sun, X. M.; Jiang, L. Superaerophobic electrodes for direct hydrazine fuel cells. *Adv. Mater.* **2015**, *27*, 2361–2366.

[63] Lu, Z. Y.; Zhu, W.; Yu, X. Y.; Zhang, H. C.; Li, Y. J.; Sun, X. M.; Wang, X. W.; Wang, H.; Wang, J. M.; Luo, J. et al. Ultrahigh hydrogen evolution performance of under-water "superaerophobic" MoS_2 nanostructured electrodes. *Adv. Mater.* **2014**, *26*, 2683–2687.

[64] Lu, Z. Y.; Li, Y. J.; Lei, X. D.; Liu, J. F.; Sun, X. M. Nanoarray based "superaerophobic" surfaces for gas evolution reaction electrodes. *Mater. Horiz.* **2015**, *2*, 294–298.